Erciyes Üniversitesi
Fen Bilimleri Enstitüsü Dergisi
Cilt 40, Sayı 2 , 2024

Erciyes University
Journal of Institue Of Science and Technology
Volume 40, Issue 2, 2024

Refractive Index Sensor and Cancer Cell Detection with Plasmonic-Based Three-Band Nearly Perfect Absorber

Ahmet Murat Erturan*[1], Seyfettin Sinan Gültekin[1]

*[1] Konya Technical University, Faculty of Engineering and Natural Sciences, Electrical-Electronics Engineering, Konya

(Alınış / Received: 03.07.2024, Kabul / Accepted: 13.08.2024, Online Yayınlanma / Published Online: 30.08.2024)

Keywords
Plasmonic biosensor, perfect absorber, refractive index sensor, cancer detection

Abstract: In this study, an antenna providing nearly perfect absorption in triple-bands operating in the mid-infrared region is proposed. The nearly perfect plasmonic absorber, featuring nanoring and nanocross antennas, demonstrated high absorption efficiencies in numerical simulations. The triple-band absorber exhibited absorption rates of 95.2%, 97.3%, and 98.1% at wavelengths of 2730 nm, 4609 nm, and 7510 nm, respectively. High absorption values explain that the localized plasmon between the dielectric and metal layers of the antenna is quite strong. These high-energy resonance modes generated by subwavelength particles enable the sensor surface to respond robustly to varying environmental conditions. The strong response highlights the capability of the sensor to detect pathogens, biomolecules, chemicals, and organisms. The variable response of each resonance mode supports the identification of biomolecules. In order to demonstrate the sensitivity of the proposed three-band perfect absorber sensor, its responses to varying refractive indices were examined, and its sensitivity was calculated. The proposed three-band perfect absorber is shown to have sensitivity values of 112.23 nm/RIU, 497.17 nm/RIU, and 841.94 nm/RIU, respectively. According to the changing refractive indices of each resonance mode, the figure of merit values was calculated as 3.67 RIU^{-1}, 1.369 RIU^{-1}, and 1.271 RIU^{-1}, respectively. The numerical results show that the sensor can detect refractive index changes sensitively. A change in the refractive index is observed between normal cells and cancer cells, and it is tested whether the sensor can detect this change. To demonstrate the sensing ability, changes in resonance modes with different cancer cells such as skin, blood, cervical, adrenal gland and lung cells were examined. The proposed nearly perfect absorber was able to detect these cancer cells at high sensitivity values of 3.67 RIU^{-1}, 1.369 RIU^{-1}, and 1.271 RIU^{-1}.

Plazmonik Tabanlı Üç Bantlı Neredeyse Mükemmel Soğurucu ile Refractive Index Sensörü ve Kanser Hücresi Algılaması

Anahtar Kelimeler
Plazmonik biyosensör, mükemmel soğurucu, kırılma indisi sensörü, kanser tespiti

Öz: Bu çalışmada, orta kızılötesi bölgede çalışan üçlü bantlarda neredeyse mükemmel soğurum sağlayan bir anten önerilmektedir. Nanohalka ve nanoçapraz antenlere sahip neredeyse mükemmel plazmonik soğurucu, sayısal simülasyonlarda yüksek soğurum verimlilikleri göstermiştir. Üçlü bant soğurucu, sırasıyla 2730 nm, 4609 nm ve 7510 nm dalga boylarında %95.2, %97.3 ve %98.1 soğurum oranları sergilemiştir. Yüksek soğurum değerleri, antenin dielektrik ve metal katmanları arasındaki yerelleşmiş plazmonun oldukça güçlü olduğunu açıklamaktadır. Alt dalga boylu parçacıklar tarafından üretilen bu yüksek enerjili rezonans modları, sensör yüzeyinin değişen çevre koşullarına güçlü bir şekilde yanıt

vermesini sağlar. Güçlü yanıt, sensörün patojenleri, biyomolekülleri, kimyasalları ve organizmaları tespit etme yeteneğini vurgular. Her rezonans modunun değişken yanıtı, biyomoleküllerin tanımlanmasını destekler. Önerilen üç bantlı mükemmel soğurucu sensörün duyarlılığını göstermek amacıyla, değişen kırılma indislerine verdiği tepkiler incelendi ve duyarlılığı hesaplandı. Önerilen üç bantlı mükemmel soğurucunun sırasıyla 112,23 nm/RIU, 497,17 nm/RIU ve 841,94 nm/RIU duyarlılık değerlerine sahip olduğu gösterildi. Her bir rezonans modunun değişen kırılma indislerine göre, değer rakamı değerleri sırasıyla 3,67 RIU^{-1}, 1,369 RIU^{-1} ve 1,271 RIU^{-1} olarak hesaplandı. Sayısal sonuçlar, sensörün kırılma indisi değişimlerini hassas bir şekilde algılayabildiğini göstermektedir. Normal hücreler ve kanser hücreleri arasında kırılma indeksinde bir değişiklik gözlemlenir ve sensörün bu değişikliği algılayıp algılayamadığı test edilir. Algılama yeteneğini göstermek için cilt, kan, servikal, adrenal bez ve akciğer hücreleri gibi farklı kanser hücreleriyle rezonans modlarındaki değişiklikler incelendi. Önerilen neredeyse mükemmel soğurucu, 3.67 RIU^{-1}, 1.369 RIU^{-1} ve 1.271 RIU^{-1} gibi yüksek hassasiyet değerlerinde bu kanser hücrelerini tespit etmeyi başarmıştır.

*İlgili Yazar, email: amerturan@ktun.edu.tr

1. Introduction

Metamaterials are artificially produced materials that show extraordinary optical characteristics [1]. Such materials are sandwich structures consisting of metal and dielectric materials with dimensions much smaller than the wavelength of light [2], [3]. Surface plasmon polaritons (SPP) propagating along these metal and dielectric surfaces exhibit extraordinary optical properties by changing the classical diffraction behavior of light [4]. While a flat metal surface reflects light strongly, a geometrically patterned metal surface exhibits intense light absorption capacity when combined with a dielectric interface [5]. A strong optical near field occurs across the metal and dielectric surface, thanks to a phenomenon called surface plasmon resonance (SPR). Moreover, patterning this metal layer with subwavelength nanoparticles reveals Localized Surface Plasmon Resonance (LSPR), resulting in tunable optical responses. In this way, light is localized around nanoparticles, creating high electrical and magnetic regions in narrow areas. The ability to manipulate light has become very popular in different fields such as biosensors [6], [7], [8], photodetectors [9], optical switches [10], optical filters [11], and photovoltaic systems [12].

Plasmonic-based structures are strong candidates for biosensing due to their advantages of strong electromagnetic surface confinement and local field enhancement [13]. Subwavelength particles not only tune the resonance mode over a wide area but also create electric and magnetic fields that are confined to the sensor surface [14], [15]. These confined and strong fields absorb a large portion of the incoming electromagnetic wave when they are compatible with the free space impedance. These high absorption points are called resonant modes. These deep dips seen at certain wavelengths are very sensitive to changes in the environment. This sensitivity exhibits a sensor behavior and gives different optical responses to changes on its surface. These features provide a significant advantage among refractive index (RI) sensors. When incident light interacts with the surface, excited plasmons produce electromagnetic fields that are highly sensitive to small changes in concentrations present at the sensor surface, causing a spectral shift in the resonance mode. Precise detection of biomolecules can be achieved with high sensitivity (S) and Figure of Merit (FoM) values based on the spectral shift occurring in the resonance mode [16], [17]. The FoM and S values are important parameters for investigating the sensitivity of the RI sensor platform and vary in direct proportion to the ability to measure RI changes. These parameters are directly affected by the metals as they are known to cause high optical losses leading to relatively broadband spectral responses [18]. It is possible to overcome this disadvantage in two ways: one way is to develop a multiband sensor platform in the mid-IR region and examine the spectral shifts in multiple resonance modes and the other way is to develop a sensor operating at the near mid-IR spectrum since the sensor shows narrow-band spectral responses at this region [19], [20].

In this study, a plasmonic near-perfect absorber nanoantenna structure with perfect absorption capacity in three different frequency bands was proposed. This absorber was configured and optimized with nanocross and a nanoring geometry to achieve a high absorption rate simultaneously in three bands. Numerical analyses revealed that the absorber showed an absorption performance of 95.2%, 97.3%, and 98.1% at wavelengths of 2730 nm, 4609 nm, and 7510 nm, respectively. The strong absorption allows the absorber to detect changes in the surface more sensitively. To demonstrate the sensing capacity based on the spectral shift, the absorber surface was coated with dielectric material with different refractive indices ranging from 1 to 1.8. The sensitivity values of the absorber at each mode are 112.23 nm/RIU, 497.17 nm/RIU, and 841.94 nm/RIU, respectively. In addition, the FoM

value of each resonance mode of the absorber was calculated as 3.67 RIU^{-1}, 1.369 RIU^{-1}, and 1.271 RIU^{-1}, respectively. The detection capability of this absorber has been tested to demonstrate its potential for detecting certain types of cancer. Cancer is a common disease worldwide and its mortality rate is quite high. A delay in diagnosing cancer significantly increases the mortality rate. In addition, the late treatment of cancer disease also leads to exposure to intense toxicity. For this reason, early diagnosis of cancer increases the chance of survival and ensures that the treatment process is completed with less damage. Additionally, some types of cancer are asymptomatic and can progress quite aggressively [21]. Therefore, frequent tests become very important for a high chance of survival. All these reasons suggest that plasmonic biosensors may be strong candidates for the detection of some types of cancer. Plasmonic biosensors facilitate molecular detection due to their sensitive, fast, and label-free detection capabilities. There are significant differences between the RI values of normal and cancerous cells in the human body. For example, the RI value was measured as 1.401 in a blood sample originating from MCF-7 breast cancer and 1.39 in a sample contaminated with T-type leukemia [22]. As an indicator of the cancer detection ability of the nearly perfect absorber platform, changes in the spectral position of each resonance mode were examined based on Basal, Jurkat, HeLa, PC-12, (MDA)-(MB)-231, MCF-7 cancer cells. The three-band resonance modes of our proposed nearly perfect absorber platform responded to each cancer cell with specific spectral shifts and demonstrated label-free detectability of these cells.

2. Materyal ve Metot

The proposed complex triple-band nearly perfect absorber structure is shown in Figure 1a. A nearly perfect absorber structure consists of metal-dielectric-metal layers. A gold material is selected for both metal layers and the dielectric plate is set for MgF_2 material. The refractive indices and dielectric constants of all materials are taken from Palik [23]. Numerical analysis of PPA was carried out using the Finite Element Difference in Time (FDTD) method. The thick Au layer at the bottom serves as an optical mirror to prevent any possible light transmission. The period of a single cell is 2600 nm for both the *x*- and *y*-axis. The thickness (t_d) of the dielectric plate between two gold layers is 150 nm. The top gold resonator is formed by placing two identical rectangles inside a ring to provide near-perfect absorption in three bands, simultaneously. The length of the nano cross is L = 1300 nm and their width is w = 200 nm. The thickness of these nano cross is optimized to t_m = 100 nm. The outer radius of a ring surrounding nano cross is determined as r_2 = 900 nm and the inner radius is determined as r_1 = 700. Therefore, as shown in Fig. 1a., the width of the Au nanoring along the ring is stabilized at 200 nm (r_2-r_1). The nanoring and nano cross resonators have 100 nm (t_m = t_d) thickness for optimum results. Numerical analyses were carried out with commercial software, Lumerical FDTD. Periodic boundary conditions along the x and y-axis and perfectly matched layer boundary conditions along the z-axis were used in the simulations. The absorption capacity of the proposed absorber can be calculated using the A(ω) formula given below in Eq. (1) [24], [25]:

$$A(\omega) = 1 - T(\omega) - R(\omega) \quad (1)$$

Here; R(ω) is the reflection, T(ω) is the transmission coefficients and A(ω) is the absorption value. The gold layer at the bottom acts as an optical mirror and prevents transmission. If the reflection is zero, the absorption goes to unity. The spectral response of reflection and absorption spectra obtained as a result of the numerical analysis of PPA is shown in Fig. 2b. It is observed that the nanoantenna demonstrates nearly-perfect absorption at λ_1 (2730 nm), λ_2 (4609 nm), and λ_3 (7510 nm) three resonance modes, simultaneously.

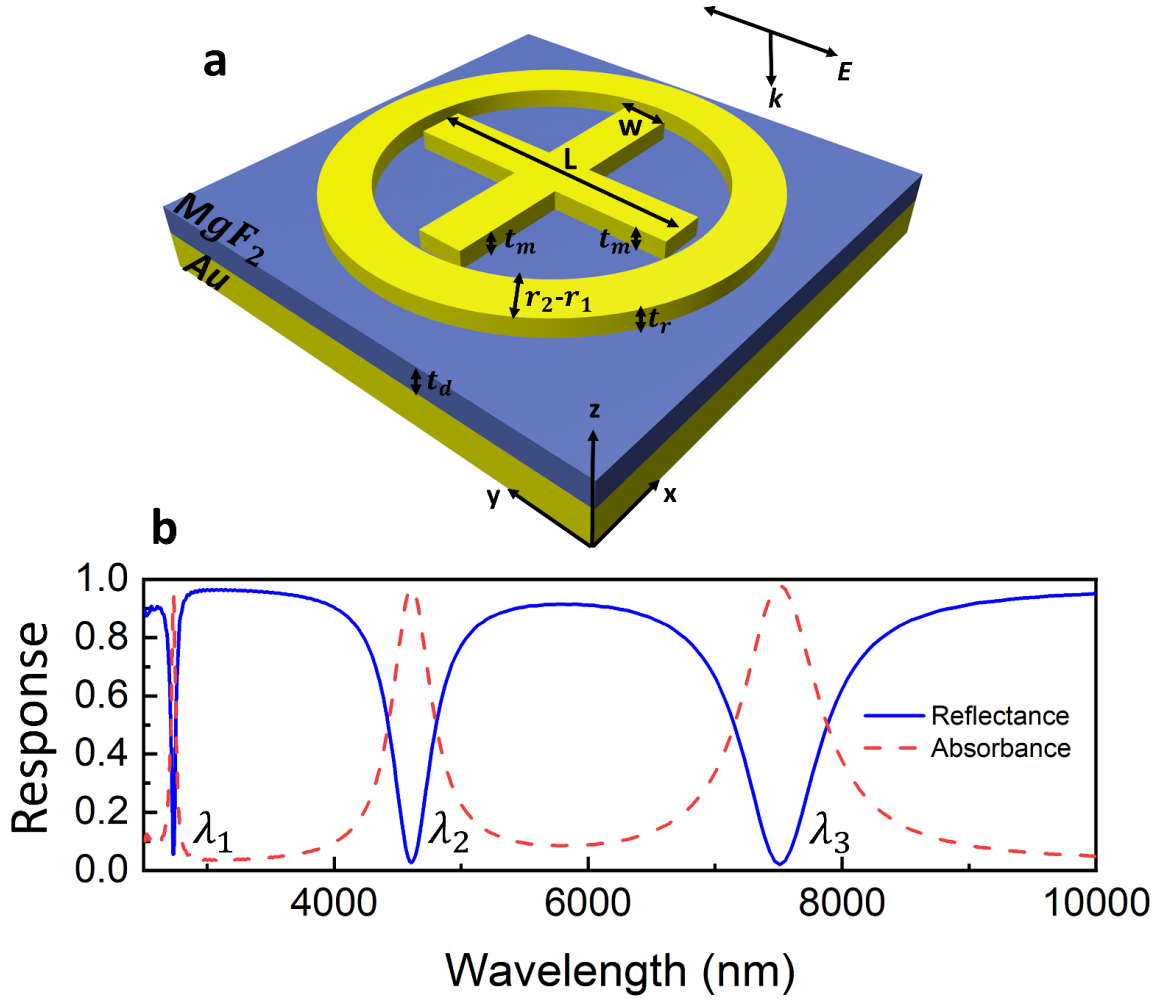

Figure 1. a. Model of the near-perfect absorber platform consisting of nanoring and nano-rectangular resonators. **b.** resonance modes of the perfect absorber platform occurring in three bands in the mid-infrared region (blue signal represents reflection, red signal represents absorption)

The resonance modes of the nearly perfect absorber consisting of nanoring and nano-rectangular resonators depend specifically on these geometries. The electric field distributions are shown in Fig. 2 to physically explain how resonance modes occur. Accordingly, the electric field distribution changes that occur during each resonance mode are shown in Fig. 2a., Fig. 2b., and Fig. 2c. According to the electric field distribution graphs, the narrow-band first resonance mode (λ_1) developed around the ring-shaped nano-antennas. The confined localized electric field distribution around ring nano-antennas is caused by plasmons oscillating between the metal and dielectric surface leading to the first resonance mode of the platform. In the second and third resonance modes, strong field enhancement is observed at the endpoints of the rectangular nano-antennas and the nanoring endpoints, respectively, lying parallel to the *x*-axis. This effect showed a dipole distribution and caused strong electric field confinement on both sides of each nanorod. A similar dipole effect was also seen at the ring ends in the final resonance mode. The gap (100 nm) between the rectangular nanorod and the nanoring enables the surface plasmons to be strongly localized and develop a strong field.

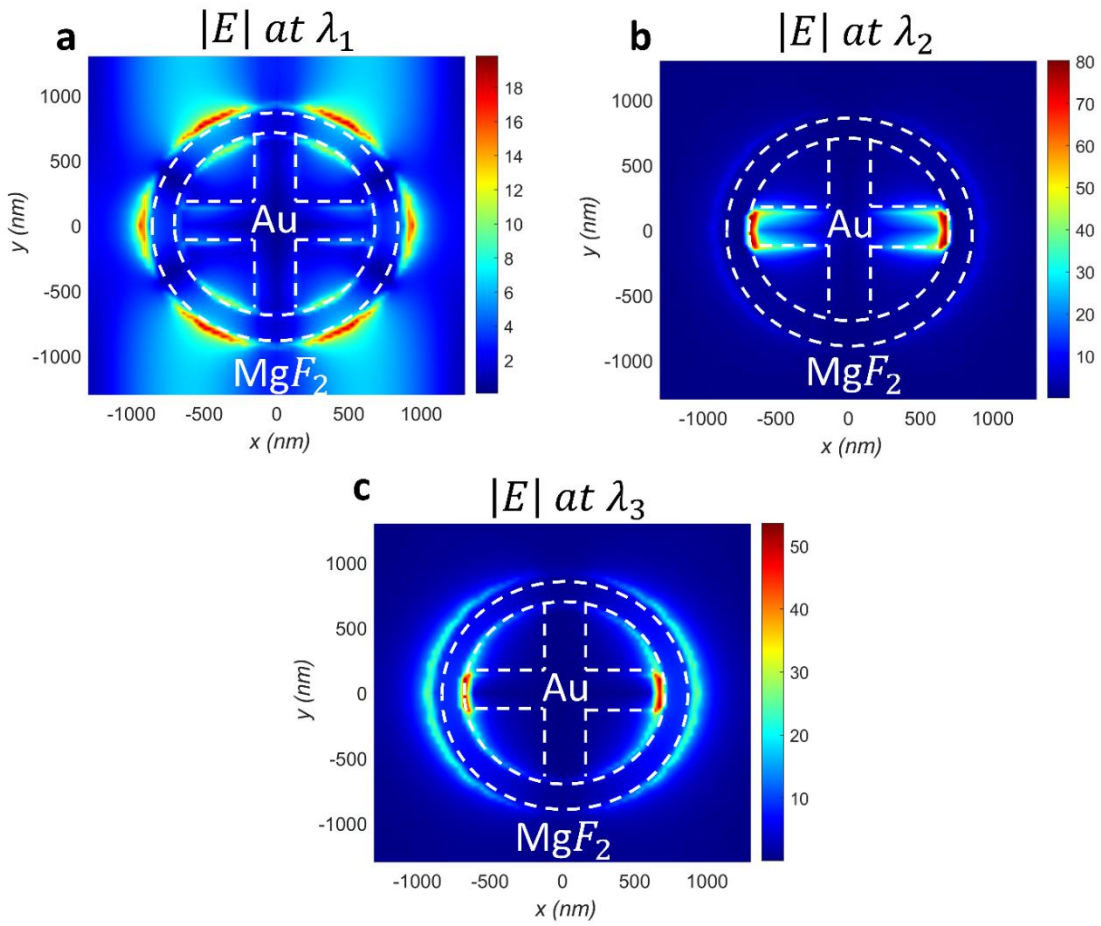

Figure 2. Electric field distribution graphs at **a.** λ_1, **b.** λ_2, **c.** λ_3 resonance wavelengths of nanoring and nano-rectangular resonators.

To more clearly analyze the dipole effect occurring in electric field distributions, the charge distributions of three different resonance modes are examined in Fig. 3. The nano ring forming the system and the two nanorods (cross-shaped) placed inside exhibit unique dipolar distributions at each mode. While the charge distributions rotating around the nanoring formed a plasmonic dipole, the nanocross inside also exhibited their own dipolar resonances. The fact that these charge distributions are drawn towards the regional endpoints of the nanorings and nanocross shows that they are structurally compatible. Fig. 3a. shows that in the first resonance mode, the charge distribution spreads throughout the nanoring and exhibits a rotating trend. Fig. 3b. clearly shows the dipole charge distribution polarized to the end regions of the nano-cross by the electric field distribution in the second resonance mode. Finally, the polarized charge distributions along the nanoring and nano cross for the third resonance mode are shown in Fig. 3c. Based on these graphs, a physical explanation of the triple resonance mode is made.

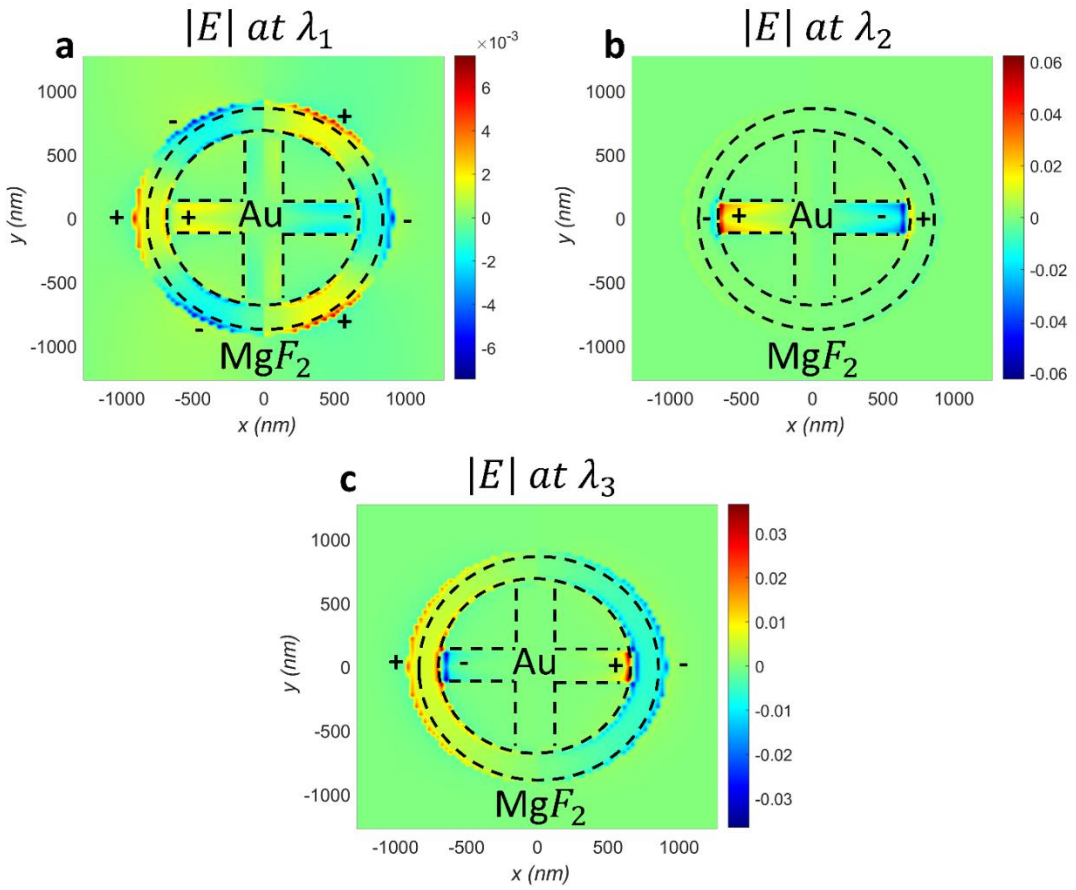

Figure 3. The charge distribution graphs at **a.** λ_1, **b.** λ_2, **c.** λ_3 resonance wavelengths of nanoring and nano-cross resonators.

3. Results

To demonstrate the RI detection ability of our proposed sensor platform based on its spectral properties, different refractive indices were examined. It is predicted that different resonance modes of the triple-band nearly perfect absorber will give different spectral responses. These spectral responses can be specifically measured and their sensitivity can be determined. High-sensitivity sensors respond to refractive index changes with a relatively larger spectral shift and shift to larger resonance wavelengths. As a result, they can detect biomolecules, proteins, chemical molecules, and different compounds, precisely. Sensitivity is one of the important factors as a measure of the detection capability of a triple-band nearly perfect absorber. The sensitivity of the sensor can be expressed as the change in wavelength per change in refractive index. To prove the sensitivity and performance of the sensor measurably, the performance of the triple-band nearly perfect absorber proposed in this study was measured by considering the RI change around it. The optical detection ability of the plasmonic RI sensor can be measured by its sensitivity (S) (Eq. (2)) [26], [27].

$$S = \frac{d\lambda}{dn} \tag{2}$$

Here, dλ value expresses the amount of spectral shift in the resonance mode. The dn value indicates the amount of RI change that causes the spectral shift. Another important parameter used to determine the sensitivity of the sensor is the Figure of Merit (FoM) value given in Eq. (3) [28], [29].

$$FoM = \frac{S}{FWHM} \tag{3}$$

Here, S denotes the sensitivity given in equation 2, while FWHM is the full width at half maximum of the resonance mode. FoM indicates how effectively the sensor can measure small changes in RI. Generally, the FoM of plasmonic sensors may be low due to the inherent losses of metals [30]. However, it is still very important to express the detection performance of these sensors quantitatively. In addition, the FoM values were measured in each resonance mode and characteristic changes were examined. Fig. 4a shows the spectral response of the proposed triple-band nearly perfect absorber to changing medium refractive indices. Refractive indices were selected with a total of 9 different values ranging from 1 to 1.8, and the spectral shifts in each resonance mode are shown for λ_1,

λ_2, and λ_3. When the refractive index of the medium was 1, the first mode captured a resonance mode at 2730 nm, the second mode at 4609 nm, and the third mode at 7510 nm wavelengths. With the increase in the refractive index of the medium, spectral shifts occurred in the λ_1 (Fig. 4b), λ_2 (Fig. 4c) and λ_3 (Fig. 4d) resonance modes, and these shifts are shown in detail for each mode.

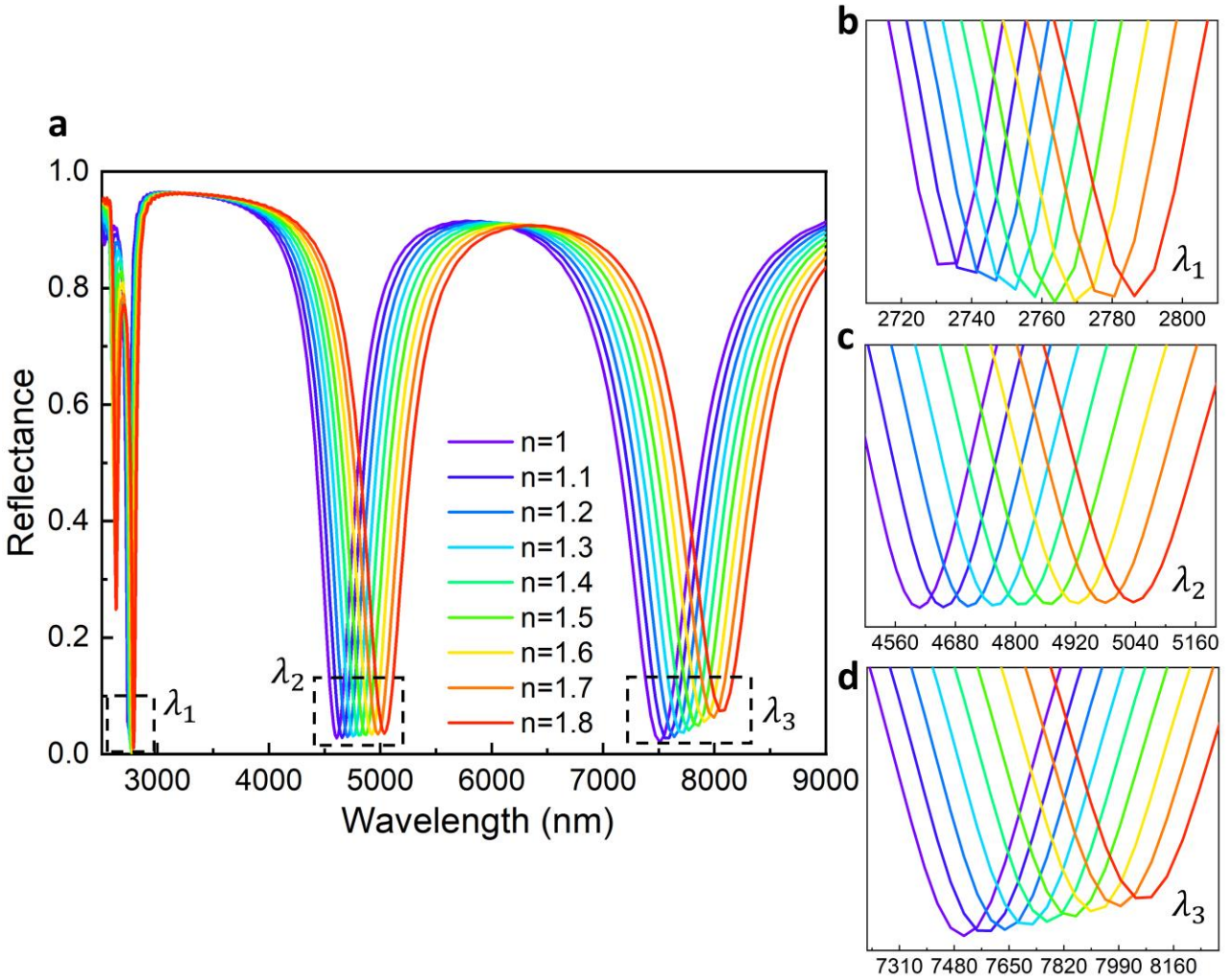

Figure 4. a. The refractive index of the surrounding medium was increased from 1.0 to 1.8, resulting in observable spectral shifts in the resonance modes of the triple-band nearly perfect absorber, specifically **b.** λ_1, **c.** λ_2, and **d.** λ_3.

The S and FoM parameters of the sensor were calculated based on the spectral shifts in the resonance mode of the triple-band nearly perfect absorber against the changing medium refractive indices. All three resonance modes are located in different wavelength regions of the mid-IR region. Resonance modes can exhibit different characteristics of the spectrum. Note that the λ_1 wavelength resonance mode is in a rather narrow band compared to the other two modes. A low FWHM value is important in the detection to have a high FoM value (Equation 3). Although the λ_2 and λ_3 resonance modes exhibit broader spectral bands, they gave significant spectral responses to varying refractive indices. Depending on the changes in the refractive index, the amount of shift in the resonance mode was examined and the sensitivity was calculated for each resonance mode of the sensor. Fig. 5 shows Wavelength shift plots occurring in three different resonance modes. When looking at all three resonance modes, it is clear that they show a linear spectral shift depending on the changing refractive index of the medium. Depending on this linear change, the sensitivities for all three modes are S1= 112.23 nm/RIU (Fig. 5a.), S2= 494.17 nm/RIU (Fig. 5b.), and S3= 841.94 nm/RIU (Fig. 5c.), respectively. The sensitivity values were calculated using Equation 2. For FoM, which is another parameter of the detection ability of the triple-band nearly perfect absorber, the FWHM values of each resonance mode were calculated and found to be 30.57 nm, 360.97 nm, and 662.42 nm, respectively. Finally, FoM values were calculated for all three resonance modes as 3.67 RIU^{-1}, 1.369 RIU^{-1}, and 1.271 RIU^{-1} for λ_1, λ_2, and λ_3, respectively. The obtained results showed the spectral responses of the medium to the changing refractive index in all three resonance modes and proved the sensitivity ability of the sensor as shown in Figure 5.

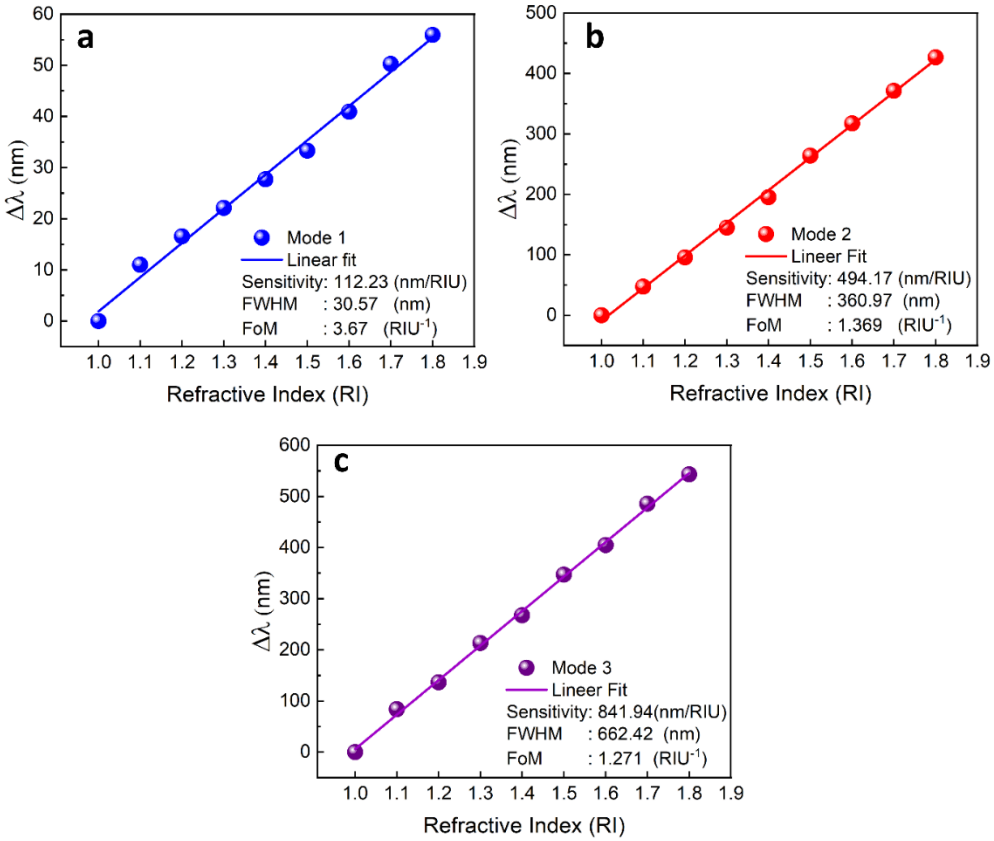

Figure 5. The variations in the three resonance modes due to changes in the refractive index of the medium are presented for **a.** λ_1, **b.** λ_2, **c.** λ_3. Additionally, the sensitivity, FWHM, and FoM values for each resonance mode are provided.

To demonstrate the detection ability of our proposed nearly perfect absorber platform, different types of cancer cells were considered, and the spectral responses of each resonance mode of the sensor were examined. The difference in concentrations of normal cells and cancer cells causes changes in the refractive indices, increasing the chances of detecting cancer cells using RI sensors. Table 1 shows the refractive indices of normal cells and cancer cells from skin, blood, cervical, adrenal gland, and lung tissues. These data were taken from references [31], [32], [33], [34] and each type of cancer cell exhibited a specific increase in refractive index due to higher protein density. Accordingly, our proposed three-band nearly perfect absorber platform was tested with both normal and cancer cells. Each of the λ_1, λ_2, and λ_3 resonance modes exhibited spectral shifts depending on the different tissues. These spectral shifts moved the resonance modes to specific spectral values, demonstrating the ability of the platform to detect cancerous cells. Each resonance mode exhibited FoM values of 3.67 RIU^{-1}, 1.369 RIU^{-1}, and 1.271 RIU^{-1}, respectively.

Table 1. Changes in resonance wavelengths for λ_1, λ_2, and λ_3 due to varying refractive indices of (a) normal and (b) cancer cells.

Cancer Type	Cell Type	Refractive Index	λ_1 (nm)	λ_2 (nm)	λ_3 (nm)
(a) Normal Cell					
Skin	Basal	1.360	2755.041	4788.221	7776.33
Blood	Jurkat	1.376	2756.786	4796.310	7789.801
Cervical	HeLa	1.368	2755.898	4792.482	7783.066
Adrenal Gland	PC-12	1.381	2757.427	4798.804	7794.011
Breast	(MDA)-(MB)-231	1.385	2757.831	4800.774	7797.379
Breast	MCF-7	1.387	2758.071	4801.768	7799.062

(b) Cancer Cell					
Skin	Basal	1.380	2757.282	4798.306	7793.163
Blood	Jurkat	1.390	2758.410	4803.255	7801.542
Cervical	HeLa	1.392	2758.636	4804.237	7803.179
Adrenal Gland	PC-12	1.395	2758.94	4805.711	7805.671
Breast	(MDA)-(MB)-231	1.399	2759.419	4807.672	7809.424
Breast	MCF-7	1.401	2759.645	4808.669	7810.958

4. Conclusions

In this study, we propose a composite nearly perfect absorber composed of nanoring and nanocross structures. The nanoscale geometry of this configuration has been optimized to support multiple resonance modes. Operating in the mid-infrared region, this structure achieved nearly perfect absorption in three distinct modes at wavelengths of 2730 nm, 4609 nm, and 7510 nm, with absorption rates of 95.2%, 97.3%, and 98.1%, respectively. The basic physical phenomena underlying the resonance modes of the plasmonic structure are explained and the sensitivity of the sensor to changing refractive indices is demonstrated. The refractive index magnitudes on the sensor surface were changed with different values between 1 and 1.8, and linear spectral shifts were observed in all three resonance modes of the sensor. The sensing capability of the sensor was analyzed by calculating the S and FoM parameters separately for each resonance mode. The results show that the λ_1, λ_2, and λ_3 resonance modes have 112.23 nm/RIU, 497.17 nm/RIU, and 841.94 nm/RIU sensitivity and 3.67 RIU^{-1}, 1.369 RIU^{-1}, and 1.271 RIU^{-1} FoM values, respectively. The λ_1 wavelength resonance signal, located at the beginning of the mid-infrared range, has a FWHM value of 30.57 nm and operates in a very narrow band. Accordingly, it responded very sensitively to changing refractive indices and enabled the sensor to have a high sensitivity value. In order to test the detection performance of the plasmonic biosensor, the changes caused by cancer cells with different refractive indices in three resonance modes were examined. For this purpose, normal and cancerous cell refractive indices of skin, blood, cervical, Adrenal Gland and lung cells were defined and tested on the sensor surface. The findings showed that all three resonance modes caused a spectral response depending on the change in cancer cells and a shift in the resonance mode occurred. These findings suggest a powerful solution to the diagnosis of cancer types whose late diagnosis is known to cause high mortality. Thanks to our proposed triple-band nearly perfect absorber, many biological and chemical molecules can be detected.

References

[1] C. W. Qiu and T. W. Odom, “Introduction: Chemistry of Metamaterials,” Chemical Reviews, vol. 122, no. 19. American Chemical Society, pp. 14987–14989, Oct. 12, 2022. doi: 10.1021/acs.chemrev.2c00541.

[2] A. K. U. Michel, “Subwavelength hybrid plasmonic structures for nonlinear nanophotonics,” Light: Science and Applications, vol. 10, no. 1. Springer Nature, Dec. 01, 2021. doi: 10.1038/s41377-021-00479-9.

[3] X. Deng, L. Li, M. Enomoto, and Y. Kawano, “Continuously Frequency-Tuneable Plasmonic Structures for Terahertz Bio-sensing and Spectroscopy,” Sci Rep, vol. 9, no. 1, Dec. 2019, doi: 10.1038/s41598-019-39015-6.

[4] S. Khani and M. Afsahi, “Optical Refractive Index Sensors Based on Plasmon-Induced Transparency phenomenon in a Plasmonic Waveguide Coupled to Stub and Nano-disk Resonators,” Plasmonics, vol. 18, no. 1, pp. 255–270, Feb. 2023, doi: 10.1007/s11468-022-01772-y.

[5] D. G. Baranov, A. Krasnok, T. Shegai, A. Alù, and Y. Chong, “Coherent perfect absorbers: Linear control of light with light,” Nature Reviews Materials, vol. 2. Nature Publishing Group, Oct. 04, 2017. doi: 10.1038/natrevmats.2017.64.

[6] S. Mostufa et al., “Metamaterial as perfect absorber for high sensitivity refractive index based biosensing applications at infrared frequencies,” J Phys D Appl Phys, vol. 56, no. 44, Nov. 2023, doi: 10.1088/1361-6463/aceb6f.

[7] A. M. Erturan, S. S. Gultekin, and H. Durmaz, “Detection of 2,4-Dinitrotoluene by Metal-Graphene Hybrid Plasmonic Nanoantennas with a Golden Ratio Rectangular Resonator,” Elektronika ir

Elektrotechnika, vol. 29, no. 3, pp. 33–38, 2023, doi: 10.5755/j02.eie.33869.
[8] A. M. Erturan, H. Durmaz, and S. S. Gültekin, "Simultaneous detection of molecules with the surface-enhanced infrared absorption sensor platform based on disk antennas with double spacer," Spectroscopy Letters, vol. 56, no. 5, pp. 283–292, 2023, doi: 10.1080/00387010.2023.2208650.
[9] J. Li et al., "Metamaterial grating-integrated graphene photodetector with broadband high responsivity," Appl Surf Sci, vol. 473, pp. 633–640, Apr. 2019, doi: 10.1016/j.apsusc.2018.12.194.
[10] T. Wang et al., "Ultrafast metamaterial all-optical switching based on coherent modulation," Opt Express, vol. 30, no. 6, p. 9284, Mar. 2022, doi: 10.1364/oe.449960.
[11] E. Ahamed, M. R. I. Faruque, M. J. Alam, M. F. Bin Mansor, and M. T. Islam, "Digital metamaterial filter for encoding information," Sci Rep, vol. 10, no. 1, Dec. 2020, doi: 10.1038/s41598-020-60170-8.
[12] M. Ossiander et al., "Metasurface-stabilized optical microcavities," Nat Commun, vol. 14, no. 1, Dec. 2023, doi: 10.1038/s41467-023-36873-7.
[13] E. Mauriz and L. M. Lechuga, "Plasmonic biosensors for single-molecule biomedical analysis," Biosensors (Basel), vol. 11, no. 4, 2021, doi: 10.3390/bios11040123.
[14] R. Yang et al., "Subwavelength optical localization with toroidal excitations in plasmonic and Mie metamaterials," InfoMat, vol. 3, no. 5. Blackwell Publishing Ltd, pp. 577–597, May 01, 2021. doi: 10.1002/inf2.12174.
[15] Y. Zhang et al., "Plasmonic tweezers: for nanoscale optical trapping and beyond," Light: Science and Applications, vol. 10, no. 1. Springer Nature, Dec. 01, 2021. doi: 10.1038/s41377-021-00474-0.
[16] V. G. Kravets, A. V. Kabashin, W. L. Barnes, and A. N. Grigorenko, "Plasmonic Surface Lattice Resonances: A Review of Properties and Applications," Chemical Reviews, vol. 118, no. 12. American Chemical Society, pp. 5912–5951, Jun. 27, 2018. doi: 10.1021/acs.chemrev.8b00243.
[17] B. Jafari et al., "Highly sensitive label-free biosensor: graphene/CaF2 multilayer for gas, cancer, virus, and diabetes detection with enhanced quality factor and figure of merit," Sci Rep, vol. 13, no. 1, Dec. 2023, doi: 10.1038/s41598-023-43480-5.
[18] L. Hajshahvaladi, H. Kaatuzian, M. Moghaddasi, and M. Danaie, "Hybridization of surface plasmons and photonic crystal resonators for high-sensitivity and high-resolution sensing applications," Sci Rep, vol. 12, no. 1, Dec. 2022, doi: 10.1038/s41598-022-25980-y.
[19] S. Yang et al., "Single-peak and narrow-band mid-infrared thermal emitters driven by mirror-coupled plasmonic quasi-BIC metasurfaces," Optica, vol. 11, no. 3, p. 305, Mar. 2024, doi: 10.1364/optica.514203.
[20] J. Kim, K. Han, and J. W. Hahn, "Selective dual-band metamaterial perfect absorber for infrared stealth technology," Sci Rep, vol. 7, no. 1, Dec. 2017, doi: 10.1038/s41598-017-06749-0.
[21] R. C. Fitzgerald, A. C. Antoniou, L. Fruk, and N. Rosenfeld, "The future of early cancer detection," Nature Medicine, vol. 28, no. 4. Nature Research, pp. 666–677, Apr. 01, 2022. doi: 10.1038/s41591-022-01746-x.
[22] M. R. Nickpay, M. Danaie, and A. Shahzadi, "Highly Sensitive THz Refractive Index Sensor Based on Folded Split-Ring Metamaterial Graphene Resonators," Plasmonics, vol. 17, no. 1, pp. 237–248, Feb. 2022, doi: 10.1007/s11468-021-01512-8.
[23] E. D. Palik, S. Diego, L. Boston, N. York, and S. T. Toronto, "Hand book of Optical Constants of Solids Edited by," 1998. [Online]. Available: http://www.apnet.com
[24] N. I. Landy, S. Sajuyigbe, J. J. Mock, D. R. Smith, and W. J. Padilla, "Perfect metamaterial absorber," Phys Rev Lett, vol. 100, no. 20, May 2008, doi: 10.1103/PhysRevLett.100.207402.
[25] Y. Xie et al., "A multifrequency narrow-band perfect absorber based on graphene metamaterial," Diam Relat Mater, vol. 137, Aug. 2023, doi: 10.1016/j.diamond.2023.110100.
[26] R. S. El Shamy, D. Khalil, and M. A. Swillam, "Mid Infrared Optical Gas Sensor Using Plasmonic Mach-Zehnder Interferometer," Sci Rep, vol. 10, no. 1, Dec. 2020, doi: 10.1038/s41598-020-57538-1.
[27] G. Lin et al., "Ultra-compact high-sensitivity plasmonic sensor based on Fano resonance with symmetry breaking ring cavity," Opt Express, vol. 27, no. 23, p. 33359, Nov. 2019, doi: 10.1364/oe.27.033359.
[28] J. Wang, Z. Xu, and D. G. Kotsifaki, "Plasmonic and metamaterial biosensors: a game-changer for virus detection," Sensors and Diagnostics, vol. 2, no. 3. Royal Society of Chemistry, pp. 600–619, May 01, 2023. doi: 10.1039/d2sd00217e.
[29] M. El barghouti, O. Haidar, A. Akjouj, and A. Mir, "Figure of merit and sensitivity enhancement of biosensor LSPR in investigated for visible and near infrared," Photonics Nanostruct, vol. 50, Jul. 2022, doi: 10.1016/j.photonics.2022.101016.

[30] Q. Duan, Y. Liu, S. Chang, H. Chen, and J. H. Chen, "Surface plasmonic sensors: Sensing mechanism and recent applications," Sensors, vol. 21, no. 16. MDPI AG, Aug. 02, 2021. doi: 10.3390/s21165262.

[31] M. A. Jabin et al., "Surface Plasmon Resonance Based Titanium Coated Biosensor for Cancer Cell Detection," IEEE Photonics J, vol. 11, no. 4, 2019, doi: 10.1109/JPHOT.2019.2924825.

[32] P. Sharma, P. Sharan, and P. Deshmukh, "A photonic crystal sensor for analysis and detection of cancer cells," 2015 International Conference on Pervasive Computing: Advance Communication Technology and Application for Society, ICPC 2015, vol. 2, no. 1, pp. 1–5, 2015, doi: 10.1109/PERVASIVE.2015.7087208.

[33] P. Kumar, Rohan, V. Kumar, and J. S. Roy, "Dodecagonal photonic crystal fibers with negative dispersion and low confinement loss," Optik (Stuttg), vol. 144, pp. 363–369, 2017, doi: 10.1016/j.ijleo.2017.06.131.

[34] K. Ahmed, B. K. Paul, F. Ahmed, M. A. Jabin, and M. S. Uddin, "Numerical demonstration of triangular shaped photonic crystal fibre-based biosensor in the Terahertz range," IET Optoelectronics, vol. 15, no. 1, pp. 1–7, 2021, doi: 10.1049/ote2.12006.